

Automated stability analysis of Piecewise affine dynamics using vertices

Pouya Samanipour and Hasan A. Poonawala

Abstract—This paper presents an automated algorithm to analyze the stability of piecewise affine (PWA) dynamical systems due to their broad applications. This paper aims to formulate the Lyapunov function as a PWA with the same polytopic regions as the PWA dynamical system. Using this formulation, Stability conditions can be expressed as linear constraints restricted by polytopes. Although linear constraints can improve the computational efficiency of the search process, the valid Lyapunov function might not be found in these polytopic regions. To overcome this challenge, a new algorithm is presented that allows the size of the parametrization of the Lyapunov function to be increased by dividing the regions during the search process. This algorithm proposes two new refinement approaches to divide each polytope into smaller ones. The first approach uses the candidate Lyapunov function, while the second uses the vector field of the PWA dynamical system in each polytope to divide it. In addition, we propose using Delaunay triangulation to manage the division of regions. To demonstrate the capabilities of the proposed algorithm, several examples involving learned models and explicit MPC controllers are presented. Examples involving learned models and explicit MPC controllers demonstrate the improved computational efficiency of the proposed algorithm when compared to mixed-integer programming methods as well as the effectiveness of determining the region of attraction.

I. INTRODUCTION

Piecewise affine (PWA) dynamical systems have gained popularity over the past few years due to their wide application in robotics [1] and the automotive industry [2]. Piecewise linear concepts are used in more advanced controllers, including gain-scheduled flight control systems [3]–[5], and Takagi-Sugeno fuzzy systems [3], [6]. We can express the closed-loop dynamics of an affine system with control saturation by PWA dynamics. Also, an effective method for synthesizing a controller for constrained linear dynamics with saturated control is using an explicit model predictive control (MPC), which can be described using a PWA dynamical model [7]. Obtaining the Lyapunov function to guarantee stability with explicit MPC could be challenging. Alternatively, there is an increasing trend in the literature to use supervised machine learning methods for learning dynamics and controllers for various applications [8], [9]. Using neural networks (NN) with ReLU activation function for learning dynamics and controller makes it possible to convert closed-loop dynamics into PWA dynamics [10]. The stability of these methods is also not guaranteed. Therefore, it is necessary to develop an automated method of finding

Pouya Samanipour and Hasan A. Poonawala are with the Department of Mechanical and Aerospace Engineering, University of Kentucky, Lexington, USA {samanipour.pouya, hasan.poonawala}@uky.edu. The corresponding author is Hasan A. Poonawala. This work is supported by the Department of Mechanical Engineering at the University of Kentucky.

the Lyapunov function for learned models, such as ReLU networks and explicit MPC.

A prevailing method for finding the Lyapunov function for PWA dynamics is sampling-based methods for learning Lyapunov function [11]–[14]. These algorithms can learn the Lyapunov function from finite samples, and they may be applied to an infinite number of input samples. As this learned Lyapunov function must meet the stability conditions at all states, verification is an integral part of the analysis. Verification can be undertaken inexactly by solving a relaxed convex problem [15], [16]. Additionally, verification can also be carried out in an exact manner using Satisfiability Modulo theories (SMT) [11], [17], [18] or Mixed-Integer Programs (MIP) [14], [19]–[21]. As a result of the exact verifier (SMT and MIP), the Lyapunov function can be certified, or a counterexample may be generated that violates the Lyapunov conditions. It is possible to add counterexamples obtained from verification to the training samples and repeat the learning process [11], [17], [18]. While numerous studies have utilized sampling-based learning for the Lyapunov function, the learning and verification approaches may be extremely cost-prohibitive due to the computational complexity of the verifiers.

Alternative to the learning approach is parameterizing the Lyapunov function and searching for the solution by forming an optimization problem [3], [22]–[24]. The Sum of Square(SOS) is used to find the Lyapunov function for nonlinear dynamics in [24]. The main challenge in SOS, however, is the complexity of computation. Parameterizing the candidate Lyapunov function as a piecewise quadratic(PWQ) is proposed in [22], [23]. Utilizing the piecewise quadratic function requires dealing with linear matrix inequalities as well as S-procedure conservatism. A less conservative approach was proposed in [22], but the results were limited to two-dimensional examples.

Instead of relying on the PWQ Lyapunov function, [3] utilized the PWA function to parameterize the Lyapunov function. An algorithm has been developed for finding a PWA Lyapunov function using partition refinement in [25]. A method for calculating the Lyapunov function for conewise PWA dynamics was proposed by [26]. The dynamics and controller of PWA have been parameterized as a ReLU in [10]. The Lyapunov function and the controller are found by parameterizing Lyapunov conditions as quantifier-free constraints for a bilinear quadratic optimization problem [10]. Although the Lyapunov condition for the PWA Lyapunov function can be expressed without conservatism, the PWQ Lyapunov function receives more attention in the literature.

This paper discusses the parameterization of the Lyapunov

function using PWA models, which enables automated search for valid Lyapunov functions through optimization. By constraining the system dynamics to polytopic regions, the affine nature of the Lyapunov function allows for stability checks on the vertices of the polytope, facilitating the use of linear programming for the search process. However, coarse partitioning of regions can lead to invalid candidate PWA Lyapunov functions. In order to overcome this problem, the paper proposes dividing each cell into smaller sub-cells so that the PWA Lyapunov function can approximate complex functions more accurately. Implementing this refinement presents challenges, especially when refined cells share edges and continuity constraints enforce the behavior of the refined cells to be similar to a single cell with the same affine Lyapunov function. Previous work [3] was limited and lacked efficacy demonstration. Furthermore, creating new regions without careful consideration may increase computational complexity. To address these challenges, this paper presents efficient cell refining methods and a suitable tool to handle the continuity problem automatically. These contributions aim to improve the refinement process and ensure the effectiveness of the refined PWA Lyapunov function.

a) Contributions: The first contribution of this paper introduces two novel methods for refining the cells in the search for valid Lyapunov functions. The first approach utilizes the derivative of the Lyapunov function as a metric to identify new vertices within each cell. The second approach involves analyzing the vector field of the PWA dynamics to identify potential new vertices in each region. By examining the behavior of the Lyapunov function or vector field, these two methods determine suitable locations for adding new vertices to the cells. Furthermore, this paper proposes the use of Delaunay triangulation as a technique to automate the refinement process for cells containing new vertices. This approach offers an effective means of refining the cells while maintaining continuity. Compared to existing refinement techniques, these methods provide the advantage of finding valid Lyapunov functions with fewer refinements. We demonstrate this by presenting non-trivial examples where the proposed search procedure successfully identifies valid Lyapunov functions within reasonable computation times. Moreover, the effectiveness of the proposed approach in determining the region of attraction (ROA) is evaluated by comparing the results with those obtained using other methods. This comparison demonstrates the capability of the proposed approach to identify the ROA using the PWA Lyapunov functions.

Following is a description of how this paper is organized. To begin with, a brief overview of the PWA and Lyapunov function parameterization is presented in Section II. In Section IV, the optimization problem to find the Lyapunov function is established, and the refinement process is presented. The results, comparisons, and limitations are provided in Section V. As a final step, the conclusion is presented.

II. PRELIMINARIES

In this paper, we examine the stability analysis problem for dynamical systems described by piecewise affine functions as follows:

$$\dot{x} = \text{PWA}(x). \quad (1)$$

where $x \in \mathbb{R}^n$ is the state variables, and term PWA denotes a piecewise affine function. We focus on continuous PWA functions with polytopic cells. In this paper, PWA Lyapunov functions are proposed as a method for analyzing stability properties of the closed-loop PWA dynamics (1). The advantage of this approach is that it enables the use of linear optimization techniques for stability analysis. In addition, this method can also be used to examine the stability of Rectified Linear Unit (ReLU) neural networks, which can be represented as PWA functions [10].

III. REPRESENTATIONS OF PIECEWISE AFFINE FUNCTIONS

This section introduces the notation for PWA functions that we use throughout the paper. We refer to the standard representation of PWA functions (see Section III-A) as an **explicit parametrization** [10].

Notation: An index for each element in the set S constitutes the set $I(S)$. The convex hull, the interior, the boundary, and the closure of the set S are denoted by $\text{conv}(S)$, $\text{Int}(S)$, ∂S , and \overline{S} respectively. The transpose of matrix A is A^T . $\langle \cdot, \cdot \rangle$ is the inner product, $\angle(\cdot, \cdot)$ is the angle between two vectors, and $|x|_2$ is the standard L_2 norm. It should be noted that the symbol \succeq implies the same element-wise rule as \geq .

Definition: In this paper, we define a partition \mathcal{P} as a collection of subsets $\{X_i\}_{i \in I(\mathcal{P})}$, where each X_i is a closed subset of \mathbb{R}^n and $\text{int}(X_i) \cap \text{int}(X_j) = \emptyset$, $\forall i, j \in I(\mathcal{P})$ and $i \neq j$. The domain of the partition, $\text{Dom}(\mathcal{P})$, is the union of all the cells in \mathcal{P} .

Given two partitions $\mathcal{P} = \{Y_i\}_{i \in I}$ and $\mathcal{R} = \{Z_j\}_{j \in J}$ of a set $S = \text{Dom}(\mathcal{P}) = \text{Dom}(\mathcal{R})$, we say that \mathcal{R} is a refinement of \mathcal{P} if $Z_j \cap Y_i \neq \emptyset$ implies that $Z_j \subseteq Y_i$. We denote the set of all refinements of \mathcal{P} as $\text{Ref}(\mathcal{P})$ [10].

A. Piecewise Affine Functions

We explicitly parameterize a piecewise affine function $\text{PWA}(x)$ by a partition $\mathcal{P} = \{X_i\}_{i \in I(\mathcal{P})}$ and a collection of matrices $\mathbf{A}_{\mathcal{P}} = \{A_i\}_{i \in I(\mathcal{P})}$ and vectors $\mathbf{a}_{\mathcal{P}} = \{a_i\}_{i \in I(\mathcal{P})}$ such that

$$\begin{aligned} \text{PWA}(x) &= A_i x + a_i, \text{ if } x \in X_i, \text{ where} \\ X_i &= \{x \in \mathbb{R}^n : E_i x + e_i \succeq 0\}. \end{aligned} \quad (2)$$

Note that a generic PWA function may not be continuous unless we appropriately constrain the parameters A_i , a_i , E_i , and e_i [3], [27]. It is assumed that any PWA function in this paper with this explicit form meets such constraints and is always continuous. Additionally, we consider the origin to be the equilibrium, thus denoting index sets I_0 and I_1 for cells with and without the origin. Also, we assume that

all the cells are bounded. Therefore, we can use the vertex representation for the PWA dynamics. Vertex is the faces of 0 dimension for the cell X_i [28] and each cell of a partition can be represented using its vertices as:

$$X_i = \text{conv}(\mathcal{F}_0(X_i)), \quad (3)$$

where $\mathcal{F}_0(X_i)$ represents a set of vertices for the cell X_i [28].

IV. MAIN ALGORITHM

In this section, first, we describe the general idea of the stability analysis and the Lyapunov function. In the next step, we parameterize the Lyapunov function as a PWA function. Then we present the stability condition for PWA dynamics with a PWA candidate Lyapunov function. In IV-C, We convert the stability analysis problem to a linear optimization problem. We construct the optimization problem to be always feasible; however, only a specific solution is accepted as a valid Lyapunov function. Furthermore, we proposed new refinement approaches IV-D to increase flexibility in the optimization process and facilitate the search for valid Lyapunov functions.

A. Lyapunov function

The Lyapunov stability theory is well known for its application to the analysis of nonlinear dynamical systems [29]. Assume that $V : D \rightarrow \mathbb{R}$ is a continuously differentiable function, and $x = 0$ is the equilibrium point of equation (1). In this case, equation (1) will be asymptotically stable if and only if V is strictly positive definite and strictly decreasing $\forall x \in D - \{0\}$.

B. PWA Lyapunov function

In the paper, we investigate the use of PWA Lyapunov functions on a bounded partition that aligns with the PWA dynamics (2) structure. This assumption can be used to further reduce computation costs by taking advantage of the convexity property. Specifically, if all cells in the partition are bounded, an affine function is considered positive on a particular cell X_i if and only if it is positive on all vertices of X_i [3]. This observation allows for simplified analysis and computation of the Lyapunov function. Consider a candidate PWA Lyapunov function such that:

$$V(x) = \begin{cases} p_i^T x + q_i & \text{for } i \in I_1 \\ p_i^T x & \text{for } i \in I_0. \end{cases} \quad (4)$$

In the equation above, the function $V(x)$ is continuous and differentiable in the interior of the cell. It is possible to calculate the derivative of the candidate Lyapunov function, along the dynamic, $\dot{x} = f(x)$, in the interior of cell $X - \{0\}$:

$$\mathcal{L}_f V = \langle \nabla V, f(x) \rangle, \quad (5)$$

where ∇V is the gradient of $V(x)$, and \mathcal{L} is the lie derivative.

When $V(x)$ is differentiable at x , let the local affine Lyapunov function be $V(x) = p^T x + q$, and the dynamics be

$\dot{x} = Ax + a$. The derivative of the Lyapunov function along the trajectories can be calculated as follows:

$$\dot{V} = p^T (Ax + a). \quad (6)$$

Lemma 4.1: Let $\{X_i\}_{i \in I}$ be a partition of a bounded subset of \mathbb{R}^n into convex polytopes with vertices v_k .

1) The Lyapunov function (4) will be positive definite iff:

$$p_i^T v_k + q_i > 0 \quad \text{for } i \in I_1, v_k \in \mathcal{F}_0(X_i) \quad (7)$$

$$p_i^T v_k > 0 \quad \text{for } i \in I_0, v_k \in \mathcal{F}_0(X_i). \quad (8)$$

2) \dot{V} , (6), will be a negative definite function iff:

$$p_i^T (A_i v_k + a_i) < 0 \text{ for } i \in I(\mathcal{P}), v_k \in \mathcal{F}_0(X_i). \quad (9)$$

Proof: These results can be derived directly as a result of parameterizing the candidate Lyapunov function in the affine form. ■

The last step is to force the Lyapunov function to be continuous. To achieve this goal, the candidate Lyapunov function (4) must meet the following requirements.

$$V_i(v_k) = V_j(v_k), \quad i \neq j \in I(\mathcal{P}), v_k \in \mathcal{F}_0(X_i) \cap \mathcal{F}_0(X_j). \quad (10)$$

Theorem 4.2: A Lyapunov function (4) in the partition \mathcal{P} is considered valid if there exist p_i and q_i satisfy (7)-(10) for every $v_k \neq 0$.

Proof: In this formulation (7)-(9) guarantees that the Lyapunov function will be positive definite. Additionally, (10) guarantees continuity. In this case, the Lyapunov function is Liptchitz continuous, but it is not differentiable at the boundary. As a result of the Liptchitz continuity of the Lyapunov function, we are able to use the Clarke generalized gradient and Clarke generalized derivative [30], [31]. According to Clarke generalized gradient $\partial V(x)$ for the PWA Lyapunov function (4) can be described as:

$$\partial V(x) = \text{conv}(\{p_i : i \in I(p), x \in X_i\}) \quad (11)$$

The Clarke generalized derivative along F for the differential inclusion $\dot{x} \in F(x)$ is provided by [30]

$$\dot{V}_F = \{p^T f : p \in \partial V(x), f \in F(x)\}. \quad (12)$$

For points $x \neq 0$ if F is a singleton function then (9) guarantees that $\dot{V}_F < 0$, $\forall p \in \partial V(x)$. As shown by [31], the maximum of the (12) upper-bounded the decrease of the Lyapunov function along solutions of the dynamical systems. Therefore, we may conclude that the Lyapunov function is decreasing along all the trajectories of the PWA dynamical systems. For more detail, please see [10]. ■

The origin is assumed always to be defined as a vertex in I_0 . The assumption that the origin is always defined as a vertex of a cell ensures that we can always find a positive-definite Lyapunov function. Another assumption is that if a vertex $v_k \in \mathcal{F}_0(X_i)$ and $v_k \in X_i \cap X_j$, then $v_k \in \mathcal{F}_0(X_j)$. This assumption is required to preserve the continuity of the Lyapunov function using (10). Details can be found in IV-D.2.

C. Optimization problem

The constraints (7)-(10) on variables p_i and q_i from (4) may be infeasible due to conditions (9) associated with the decrease of the Lyapunov function along solutions. Slack variables are added to these constraints to ensure feasibility. Consequently, we can formulate the search process for the PWA Lyapunov function as follows:

$$\min_{p_i, q_i, \tau_i} \sum_{i=1}^N \tau_i \quad (13)$$

Subject to:

$$\begin{aligned} p_i^T (A_i v_k + a_i) - \tau_i &< -\epsilon_1 \quad \forall i \in I_1, v_k \in \mathcal{F}_0(X_i) \\ p_i^T A_i v_k - \tau_i &< -\epsilon_1 \quad \forall i \in I_0, v_k \in \mathcal{F}_0(X_i) \\ p_i^T v_k + q_i &> \epsilon_2 \quad \forall i \in I_1, v_k \in \mathcal{F}_0(X_i) \\ p_i^T v_k &> \epsilon_2 \quad \forall i \in I_0, v_k \in \mathcal{F}_0(X_i) \\ V_i(v_k) &= V_j(v_k) \quad \forall v_k \in \mathcal{F}_0(X_i) \cap \mathcal{F}_0(X_j), i \neq j \\ \tau_i &\geq 0 \quad \forall i \in I(\mathcal{P}) \end{aligned}$$

where τ_i is the slack variable associated to cell X_i , and $\epsilon_1, \epsilon_2 > 0$. By design, we can state the following result.

Lemma 4.3: The optimization problem in (13) is always feasible.

Proof: This result is by the construction of the optimization problem. ■

The solution to this optimization problem yields a valid Lyapunov function if and only if all the slack variables are zero. If the cost function is non-zero, the Lyapunov function is non-decreasing at some vertices. In fact, no Lyapunov function associated with the current partition exists. It may be possible to refine the partition, meaning to divide regions within it, in order to increase the capacity of the Lyapunov function and then repeat the search using this higher-capacity function. In the following section, the refinement process is described in detail.

D. Refinement

A refinement of the current partition is intended to enhance the flexibility of the Lyapunov function search process. To achieve flexibility, a cell X_i with a nonzero slack variable will be divided into smaller sub-cells. In order to keep things simple, we assume that the refinement of X_i will result in the creation of two new subcells, X_{i_1} and X_{i_2} . For each subcell, we can parameterize the PWA Lyapunov function as $V_{i_1} = p_{i_1}^T x + q_{i_1}$ and $V_{i_2} = p_{i_2}^T x + q_{i_2}$. As a result, the candidate Lyapunov function for cell X_i has a higher capacity PWA function that is more flexible. Furthermore, the new PWA Lyapunov function has more parameters, p_i and q_i , as well as constraints. Increasing the number of parameters and constraints might increase the computational complexity for solving (13) since the computational complexity of linear optimization with n parameters and accuracy parameter ϵ is $O(n^{3/4} \log(\frac{n}{\epsilon}))$ [32]. Therefore, to implement refinement, it is necessary to use an intelligent approach, since otherwise, the complexity of the computation may increase.

We utilize a vertex representation for the refinement process to represent cells within a partition, which are convex polytopes. The process of refinement for cells involves adding a new vertex on the cell's boundary and then forming new sub-cells. For this section, we will begin by defining a few concepts and definitions that will be useful for describing these two steps. The first concept is the **simplex region**, a bounded region with the smallest possible number of vertices in \mathbb{R}^d . Polytope's faces of dimension one are called **edges** [28]. In cell X_i , we define the edges by the set $\mathcal{F}_1(X_i)$, and each edge is represented by a pair of vertices (v_j, v_k) , where $v_j, v_k \in \mathcal{F}_0(X_i)$. The edges of convex polytopes can be obtained by using MILP as described in [33]. It is worth emphasizing that the edges containing the origin, where $v_j = 0$ or $v_k = 0$, are not taken into account in the set of edges $\mathcal{F}_1(X_i)$. By making this assumption, we ensure that refinement will not be applied to edges containing the origin. Therefore, if $X_i \in I_0$, its subcells will always contain the origin after refinement.

For the cell X_i , with dynamic $\dot{x} = A_i x + a_i$ and the candidate Lyapunov function $V_i = p_i^T x + q_i$ we can define the following sets and functions.

- 1) We can find the vector field and the derivative of the Lyapunov function at a vertex, v_j , using the following functions.

$$\dot{x}(X_i, v_j) = A_i v_j + a_i, \quad (14)$$

$$\dot{V}(X_i, v_j) = p_i^T \dot{x}(X_i, v_j), \quad (15)$$

where $\dot{x}(X_i, v_j) \in \mathbb{R}^n$ is the vector field of the local dynamic at the vertex v_j , and $\dot{V}(X_i, v_j)$ is the derivative of the Lyapunov function at the specified vertex in X_i .

- 2) The vertices of the longest edge of a cell can be obtained using the following function:

$$L_{max}(i) = \operatorname{argmax}_{(v_j, v_k) \in \mathcal{F}_1(X_i)} (|v_j - v_k|_2) \quad (16)$$

- 3) The following function can be used to capture changes in the sign of the derivative of a candidate Lyapunov function:

$$sgn_{\dot{V}}(i) = \begin{cases} 1 & \operatorname{sgn}(\dot{V}(X_i, v_j)) \geq 0, \forall v_j \in \mathcal{F}_0(X_i), \\ -1 & \operatorname{sgn}(\dot{V}(X_i, v_j)) \leq 0, \forall v_j \in \mathcal{F}_0(X_i), \\ 0 & \text{otherwise,} \end{cases} \quad (17)$$

where the $\operatorname{sgn}(x)$ is the standard sign function. This function generates zero whenever the sign of the derivative of the candidate Lyapunov function in the cell X_i changes. Otherwise, this function generates either 1 or -1 depending on the sign of the derivative of the candidate Lyapunov function within the cell X_i .

- 4) With $sgn_{\dot{V}}(i)$ being 0, the following set may also be used to provide the vertices of the edges where the sign of the derivative of the Lyapunov function has

Algorithm 1 Finding new vertices using naive refinement

Require: PWA(x), Vertices

1- Find

$$i = \operatorname{argmax}_{i \in I_s} (\tau_i) \quad (22)$$

2- Find (v_j, v_k) using $L_{max}(i)$ (16).

3- finding v_{new_i} using (21) where $\alpha = \beta = 0.5$.

return v_{new_i}, i .

changed.

$$c_V(i) = \{(v_j, v_k) : sgn_{\dot{V}}(i) = 0, \forall (v_j, v_k) \in \mathcal{F}_1(X_i), \dot{V}(X_i, v_j)\dot{V}(X_i, v_k) < 0\}. \quad (18)$$

There are multiple edges where the sign of the derivative of the Lyapunov function has changed if $sgn_{\dot{V}}(i) = 0$.

5) The following equation can be used to determine the vertices for an edge with the largest variation in the derivative of a candidate Lyapunov function.

$$\Delta \dot{V}_{max}(i) = \{(v_j, v_k) : \operatorname{argmax}_{(v_j, v_k) \in \mathcal{F}_1(X_i)} |\dot{V}(X_i, v_j) - \dot{V}(X_i, v_k)|\}. \quad (19)$$

6) We aim to determine the edge along which the vector fields exhibit the greatest range of angle variations. Therefore, we use the following function to find the edge with the smallest cosine between the vector field at its vertices.

$$\cos_{min}(i) = \{(v_j, v_k) : \arg \min_{(v_j, v_k) \in \mathcal{F}_1(X_i)} \frac{\langle \dot{x}(X_i, v_j), \dot{x}(X_i, v_k) \rangle}{|\dot{x}(X_i, v_j)|_2 |\dot{x}(X_i, v_k)|_2}\}. \quad (20)$$

Now, we can delve into the refinement process.

1) *Finding new vertices:* The first step in the refinement process is to introduce new vertices on the boundary of cells in $I_s = \{i \in I : \tau_i > 0\}$. The new vertex for the cell X_i can be obtained using the following equation:

$$v_{new_i} = \alpha v_j + \beta v_k, \quad (21)$$

which is a linear combination of two vertices of an edge. Based on the splitting approach which will be introduced in this section, α, β, v_j , and v_k in (21) could be different. Here we consider three different approaches for finding the new vertices.

a) *Naive refinement:* The first algorithm is inspired from [3]. The original algorithm was described for simplex regions and restricted to 2-D problems. In order to make the comparison possible we generalize the method for all types of regions. The process of refinement for the cell X_i based on [3] is described in **Algorithm 1**. The naive algorithm adds a new vertex exclusively to the longest edge, denoted as L_{max} , of cell X_i that has the largest slack variable, as determined by (22). This method creates sub-cells with the

Algorithm 2 Finding new vertices using Lyapunov-based refinement

Require: PWA(x), Vertices

for $i \in I_s$ **do**

1- Finding $sgn_{\dot{V}}(i)$ using (17).

if $sgn_{\dot{V}}(i) = 0$ **then**
for $(v_j, v_k) \in c_V(i)$ **do**

1- Solve the convex problem (23) to obtain α and β .

2- Find v_{new_i} using (21).

end for
else

1- Find (v_j, v_k) using $\Delta \dot{V}_{max}(i)$ (19).

2- Find v_{new_i} using (21) where $\alpha = \beta = 0.5$.

end if
end for
return v_{new_i}, i .

largest possible volume without considering the candidate Lyapunov function or local dynamics. Consequently, it may lead to unsatisfactory results. Selecting vertices randomly could increase computational complexity without necessarily improving the refinement process. Thus, it is crucial to choose new vertices intelligently.

b) *Lyapunov-based refinement:* To address the challenge with the naive refinement, a new approach is proposed, leveraging the candidate Lyapunov function to make more informed decisions regarding selecting new vertices. The basic principle behind this method is that for every cell X_i where $i \in I_s$ finding a set of points $P(i) = \{v_{new_i} : \dot{V}(X_i, v_{new_i}) = 0, v_{new_i} \in \partial X_i\}$. Using these points, $v_{new_i} \in P(i)$, the cell X_i could be divided into the two sub-cells, X_{i_1} and X_{i_2} , where $sgn_{\dot{V}}(i_2) = -sgn_{\dot{V}}(i_1)$. In the case of $sgn_{\dot{V}}(i) = 0$, we know that $P(i) \neq \emptyset$. Therefore, we can find these points using the following convex problem in cell X_i .

$$\begin{aligned} & \max_{\alpha, \beta} 0 \\ \text{s.t.} \quad & \alpha \dot{V}(X_i, v_j) + \beta \dot{V}(X_i, v_k) = 0, \\ & \alpha + \beta = 1, \\ & 0 \leq \alpha, \beta \leq 1, \\ & (v_j, v_k) \in \mathcal{F}_1(X_i). \end{aligned} \quad (23)$$

An explanation of how to find i, v_j and v_k in (23) and other details about finding a new vertex using Lyapunov-based refinement can be found in **Algorithm 2**. If $sgn_{\dot{V}}(i) = 1$, then $P(i) = \emptyset$, so we choose the new vertex at the edge obtained from $\Delta \dot{V}_{max}(i)$.

In contrast to the previous method that focused only on the cell with the largest slack variable, the Lyapunov-based refinement is now applied to all cells with nonzero slack variables, denoted as $i \in I_s$. As a result of this broader approach, each relevant cell will be refined based on its individual candidate Lyapunov function. However, it

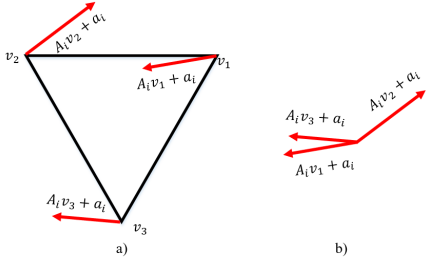


Fig. 1. Vector fields of a cell on its vertices. b) The angle between vector fields of vertices. As can be seen, the angle of the vector field between v_1 and v_2 is close to $-\pi$.

Algorithm 3 Finding new vertices using Vector field refinement

Require: PWA(x), Vertices

```

for  $i \in I_s$  do
    1- Find  $(v_j, v_k)$  using (20).
    2- Find  $\alpha$  and  $\beta$  using following equation:
        
$$\alpha = \frac{1}{1 + \frac{|\dot{x}(X_i, v_j)|_2}{|\dot{x}(X_i, v_k)|_2}}, \beta = 1 - \alpha.$$
 (24)
end for
return  $v_{new_i}, i.$ 

```

is important to note that the coefficient vector p_i used in the refinement process may change significantly in the next iteration. Therefore, this approach may not be suitable in all cases, as the optimization process in the subsequent steps can alter the candidate Lyapunov function.

c) *Vector field refinement*: To address the problem with the Lyapunov-based refinement, the search for new vertices should be conducted using a method that is not influenced by the optimization process in the subsequent steps. The proposed method leverages the vector field information of the dynamics, which remains unchanged during the optimization process. The underlying heuristic behind this method is that the direction or magnitude of the vector fields along an edge may undergo significant changes within a cell X_i where $i \in I_s$. Consequently, a higher-capacity PWA function may be required to represent the Lyapunov function within X_i accurately. As illustrated in Fig.1, the vector field direction in a cell can exhibit substantial variations, such as a flip from v_1 to v_2 . In such cases, a simple PWA function may struggle to approximate the level set accurately. To mitigate this, the method is adding a new vertex, v_{new_i} , between (v_1, v_2) where $\angle(\dot{x}(X_i, v_1), \dot{x}(X_i, v_{new_i})) = \angle(\dot{x}(X_i, v_2), \dot{x}(X_i, v_{new_i}))$. Consequently, after each refinement process, the greatest angle between the vector fields of an edge in cell X_i is divided in half. The process of finding a new vertex using the vector field refinement is outlined in **Algorithm 3**, which provides a detailed description of the method.

Before moving on to the next step, storing the new vertices created by these algorithms in the following buffer

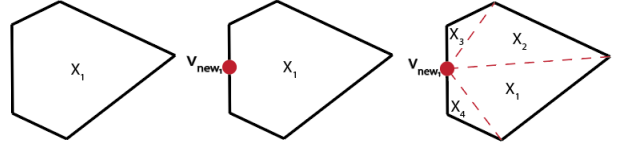


Fig. 2. Triangulation process using Delaunay. a) A non-simplex region b) Midpoint is chosen to be added as a new vertex. c) The refined cells generated by the Delaunay triangulation.

is necessary.

$$B = \{v_{new_i} \in \mathbb{R}^n : i \in I_s\}. \quad (25)$$

Now we can proceed to the next step, which is forming sub-cells.

2) *Forming sub-cells*: In order to form sub-cells, Johannson [3] proposed remedies for 2-D systems; however, this method is limited to simplex cells. It was suggested that triangulation methods be used for non-simplex regions in [3], but no specific method or implementation is presented. It has also been proposed in [34] to apply Delaunay triangulation to all cells; however, the results have been limited to 2-D examples. We apply Delaunay triangulation to overcome the challenges associated with forming sub-cells for non-simplex cells and cells in higher dimensions ($n > 2$), which would be challenging to accomplish manually.

The Delaunay triangulation of a set of points in \mathbb{R}^d is defined to be the triangulation such that the circumcircle of every triangle in the triangulation contains no point from the set in its interior. Such a unique triangulation exists for every point set in \mathbb{R}^d , and it is the dual of the Voronoi diagram. Moreover, the Delaunay triangulation will maximize the minimum angle in each triangle [35]. $DT(\mathcal{F}_0(X_i))$ is the notation for implementing Delaunay triangulation using the vertices of the cell X_i . The process of implementing Delaunay triangulation for a single cell is illustrated in Fig.2. Delaunay triangulation will also handle the continuity of the Lyapunov function if the partition is composed of multiple cells. To illustrate how continuity is preserved, let us consider the v_{new_i} as the new vertex obtained using (21) for the cell X_i . If $v_{new_i} \in X_i \cap X_j$, then v_{new_i} must also be considered as a new vertex for the cell X_j , and $DT(\mathcal{F}_0(X_i) \cup v_{new_i})$ and $DT(\mathcal{F}_0(X_j) \cup v_{new_i})$ should be implemented. Consequently, even after refinement, continuity would be guaranteed by (10). Generally, in order to implement Delaunay triangulation within the current partition, we have to follow the following steps.

1) First, we must obtain the following set containing cells that required refinement.

$$I_{split} = \{i : X_i \cap B \neq \emptyset, i \in I(\mathcal{P})\}. \quad (26)$$

2) Then, we need to find the vertices located on the boundary of the cell X_i where $i \in I_{split}$ using the

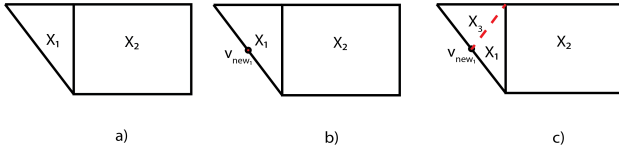


Fig. 3. The process of refinement using naive refinement a) Two adjacent cells where $\tau_1 > \tau_2 > 0$. b) Based on the naive refinement method, the new vertex is located on the longest edge of the cell X_1 because it has the greatest slack variable τ_1 . c) Delaunay triangulation is used to form the sub-cells.

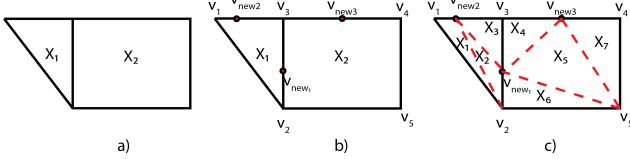


Fig. 4. The process of refinement using Lyapunov-based refinement a) Two adjacent cells where $\tau_1 > \tau_2 > 0$. b) Let's assume in the simplex cell, X_1 , we have $\dot{V}(X_1, v_2) < 0 < \dot{V}(X_1, v_1) < \dot{V}(X_1, v_3)$ and in the non-simplex-cell, X_2 , $0 < \dot{V}(X_2, v_3) < \dot{V}(X_2, v_2) < \dot{V}(X_2, v_5) < \dot{V}(X_2, v_4)$. Based on the Lyapunov-based refinement method, the new vertices, v_{new1} and v_{new2} , for the simplex cell will be obtained using (23) on the edges obtained using (18). For the non-simplex cell, the new vertex v_{new3} is obtained using (21) where $\alpha = \beta = 0.5$ on the edge obtained using (19) c) Delaunay triangulation is used to form the sub-cells for the cell X_1 and X_2 with their new vertices. Delaunay Triangulation for the cell X_1 and X_2 will be $DT(F_0(X_1) \cup v_{new1} \cup v_{new2})$ and $DT(F_0(X_2) \cup v_{new1} \cup v_{new3})$ respectively.

following set.

$$\mathcal{V}_{new}(i) = \{v_{new_j} : v_{new_j} = X_i \cap B, i \in I_{split}\}. \quad (27)$$

3) Then, we can form the new sub-cells using $DT(F_0(X_i) \cup \mathcal{V}_{new}(i))$ for $i \in I_{split}$.

The process of refinement based on the naive approach using Delaunay triangulation is shown in Fig. 3. As can be seen, the sub-cells are created just in the simplex cells. However, the Lyapunov-based and vector-field methods perform differently as shown in Fig.4. and Fig.5. respectively.

E. Stability Analysis Algorithm

This section provides a detailed description of the stability analysis algorithm. The algorithm begins by solving the

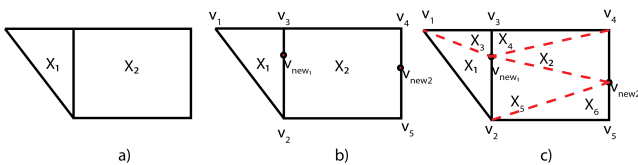


Fig. 5. The process of refinement using vector field refinement a) Two adjacent cells where $\tau_1 > \tau_2 > 0$. b) Let's assume in the simplex cell we have the biggest variation in the vector field angle, $\cos_{min}(1) = (v_2, v_3)$, and in the non-simplex cell the biggest variation of the vector field, $\cos_{min}(2) = (v_4, v_5)$. Based on the vector field refinement method, the new vertex for the simplex and non-simplex cell will be obtained using (21) with α and β obtained from (24). c) The Delaunay triangulation is employed to form the sub-cells for the cell X_1 and X_2 using $DT(F_0(1) \cup v_{new1})$ and $DT(F_0(2) \cup v_{new1} \cup v_{new2})$ respectively.

Algorithm 4 Verifying Stability using Vertices

Require: PWA(x), Vertices

Solve Optimization Problem (13) with the initial PWA dynamics.

while $\sum_{i=1}^N \tau_i \neq 0$ **do**

for $i \in I_s$ **do**

 1- Finding new vertices using presented methods(see IV-D.1).

 2- Add the new vertex to B (25).

end for

for $i \in I_{split}$ **do**

 1- Finding set of vertices $\mathcal{V}_{new}(i)$ for cell X_i .

 2- Forming sub-cells $DT(F_0(X_i) \cup \mathcal{V}_{new}(i))$ (see (IV-D.2)).

end for

Solve Optimization Problem (13) with the refined PWA dynamics.

end while

return $V(x) = p_i^T x + q_i \quad \forall i \in I(\mathcal{P})$.

optimization problem specified in Equation (13) using the initial partitions. If the cost function is non-zero, indicating that a valid Lyapunov function has not been found, the refinement process described in Section IV-D is applied. This iterative process is repeated multiple times until a valid Lyapunov function is determined. To facilitate a better understanding of the algorithm, a pseudo-code representation is presented in **Algorithm 4**. This algorithm will continue iterating until a solution is found, ensuring that the search for a valid Lyapunov function is exhaustive.

V. RESULTS

The paper presents six examples to demonstrate the search performance for a PWA Lyapunov function using the algorithm described in **Algorithm 4**. The computations are implemented using the Mosek optimization package [36] and Python 3.9 on a computer with a 2.1 GHz processor and 8 GB RAM. During the computations, a tolerance of 10^{-8} is used to determine if a number is nonzero. In all the examples, the values of ϵ_1 and ϵ_2 are set to 10^{-4} . These examples aim to showcase the effectiveness and efficiency of the proposed algorithm in finding valid Lyapunov functions within reasonable computation times.

Example 1 (Multi-agent consensus): The Hegselmann-Krause model is a widely studied model in the literature, which involves N autonomous agents with state variables ξ_i . Each agent's dynamics are given by the equation:

$$\dot{\xi}_i = \sum_{j=1}^N \phi(\xi_i, \xi_j)(\xi_j - \xi_i) \quad (28)$$

where i ranges from 1 to N , and $\phi : [0, 1]^2 \rightarrow \{0, 1\}$ represents a weight function as defined in the reference [22]. The stability analysis results for this model are presented in Figure 6. We observed that a valid PWA Lyapunov function

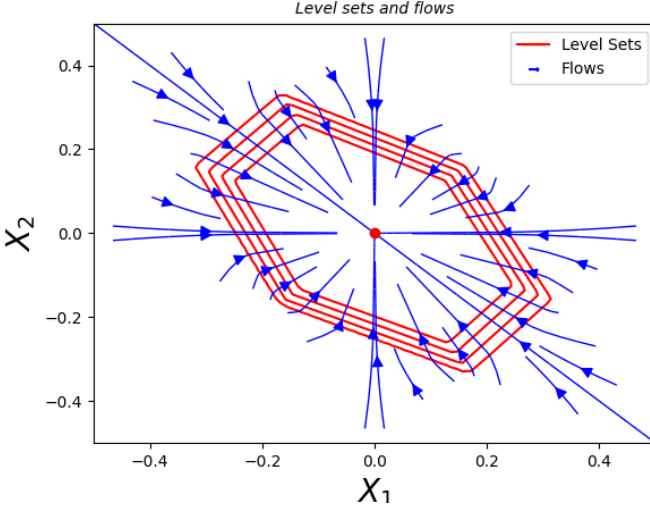


Fig. 6. Selected level sets and flows for the Example 1.

can be obtained without requiring any refinement. Therefore, the choice of different splitting approaches does not have any impact on this particular example. The details are provided in TableI.

Example 2 (2-D example from [30], [26], [3]): This system has been presented in four different regions as follows:

$$\begin{aligned} Z_1 &= \{x \in \mathbb{R}^2 : -x_1 + x_2 \geq 0, x_1 + x_2 \geq 0\} & (29) \\ Z_2 &= \{x \in \mathbb{R}^2 : -x_1 + x_2 \geq 0, -x_1 - x_2 \geq 0\} \\ Z_3 &= \{x \in \mathbb{R}^2 : x_1 - x_2 \geq 0, -x_1 - x_2 \geq 0\} \\ Z_4 &= \{x \in \mathbb{R}^2 : x_1 - x_2 \geq 0, x_1 + x_2 \geq 0\} \end{aligned}$$

and the dynamics are as follows:

$$\Omega_p : \dot{x} = \begin{cases} \begin{bmatrix} -0.1 & 1 \\ -5 & -0.1 \end{bmatrix} x & \text{if } x \in Z_1 \text{ or } x \in Z_3 \\ \begin{bmatrix} -0.1 & 5 \\ -1 & -0.1 \end{bmatrix} x & \text{if } x \in Z_2 \text{ or } x \in Z_4. \end{cases} \quad (30)$$

The level sets and the vector fields are shown in Fig.7. The PWA Lyapunov function was obtained by refining the cells. In this example, all three refinement methods perform similarly in finding the Lyapunov function. The details about this example are presented in TableI. The refinement process creates 128 cells in the partition.

Example 3 (Explicit model-predictive controller [10]): In this study, the stability of the following discrete time dynamic is investigated using explicit MPC, similar to [10], [19].

$$x_{t+1} = \begin{bmatrix} 1 & 1 \\ 0 & 1 \end{bmatrix} x_t + \begin{bmatrix} 1 \\ 0.5 \end{bmatrix} u_t \quad (31)$$

As in [10], the MPC problem has the same specification such as stage cost, actuator, and state constraints. We use the MPT3 toolbox [37] in Matlab to obtain an explicit controller. A sampling time of $t_s = 0.01s$ was used to

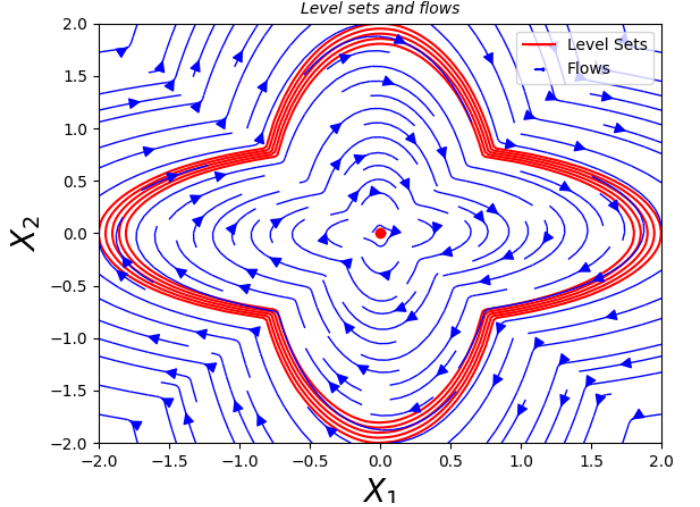


Fig. 7. Selected level sets and flows of the Example 2.

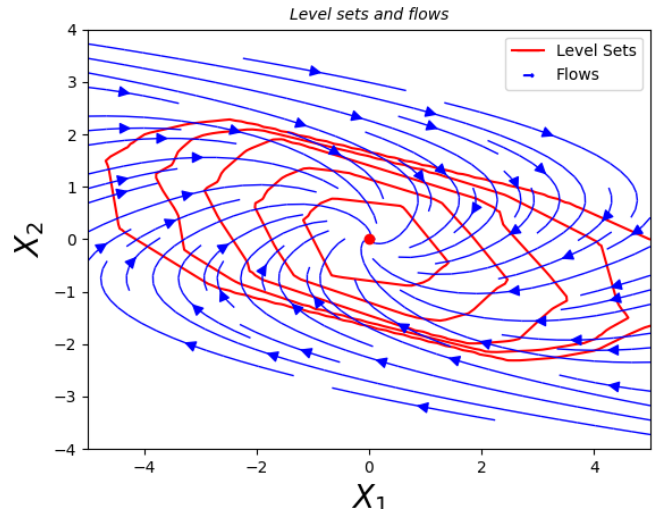


Fig. 8. Selected level sets and flows for the Example 3.

obtain the continuous form of the dynamic (31) with the explicit MPC controller. The PWA dynamics generated by the explicit MPC have a cell where the origin is not on the vertices. As a result, we refine this cell with the origin as a new vertex, $DT(\mathcal{F}_0(X_i) \cup 0)$, and then start the **Algorithm 4**. Fig.8. depicts the level sets of the Lyapunov function. The Lyapunov function was found by all three refinement algorithms within one second. The Lyapunov-based refinement and the vector-field refinement, however, produce a greater number of cells than the naive refinement. The performance of all refinement methods in 2-D seems to be similar so far. In the next example, we will evaluate refinement methods using a 4-D example.

Example 4 (4-D Example [19]): For this example, we

will use the 4-D MPC example presented in [19] as follows:

$$x_{t+1} = \begin{bmatrix} 0.4346 & -0.2313 & -0.6404 & 0.3405 \\ -0.6731 & 0.1045 & -0.0613 & 0.3400 \\ -0.0568 & 0.7065 & -0.086 & 0.0159 \\ 0.3511 & 0.1404 & 0.2980 & 1.0416 \end{bmatrix} x_t + \begin{bmatrix} 0.4346 \\ -0.6731 \\ -0.0568 \\ 0.3511 \end{bmatrix} u_t. \quad (32)$$

It includes the same details as [19], such as a state constraint of $\|x\|_\infty \leq 4$, an input constraint of $\|u\|_\infty \leq 1$, a prediction horizon of $T = 10$, a stage cost of $Q = 10I$ and $R = 1$. Explicit MPC produces a PWA dynamic with 193 cells. To ensure that the origin is a vertex, we refined the cell with the origin on its interior first. Our next step is to convert the discrete-time PWA dynamics into continuous-time PWA dynamics with a sampling time $t_s = 0.01$. Finally, We searched for the continuous PWA Lyapunov function using **Algorithm 4** with all refinement techniques. The Mosek became stuck after 31 iterations with naive refinement. **Algorithm 4** found the Lyapunov function in 1200 seconds using the Lyapunov-based refinement with 5874. With the vector field refinement, the **Algorithm 4** found the solution in 280 seconds by generating 3086 cells. In comparison with [19], the Lyapunov function using vector-field refinement requires a shorter computational time.

Example 5 (Inverted Pendulum [10], [14], [17]): It is common in the literature to use an inverted pendulum as an example with the following state-space model:

$$\begin{bmatrix} \dot{x}_1 \\ \dot{x}_2 \end{bmatrix} = \begin{bmatrix} x_2 \\ -\frac{c}{m}x_2 - gl^2 \sin(x_1) \end{bmatrix} + \begin{bmatrix} 0 \\ \frac{1}{ml^2} \end{bmatrix} u \quad (33)$$

where $m = 0.15$ kg, $l = 0.5$ m, $c = 0.1Ns/rad$, and $g = 9.81$ m/s² [18]. First, we used a single-hidden layer ReLU neural network consisting of 20 neurons in the region $\|x\|_\infty \leq 4$ to identify the uncontrolled dynamics. Subsequently, we designed a ReLU neural network controller as described in [10]. By incorporating the ReLU NN controller into the system, we were able to achieve stability. We searched for the PWA Lyapunov function using **Algorithm 4** with the Vector-field refinement. The results are compared with Linear-quadratic regulator (LQR) [17] and NN Lyapunov function [18] in Fig.9. The Lyapunov function obtained using the proposed approach has a larger ROA. It is important to note that the valid region for [17] and [18] is $\|x\|_2 \leq 4$.

Example 6 (Path Following Wheeled Vehicle [18]):

The following kinematic model is used to analyze the stability of a path following wheeled vehicle in [18]:

$$\begin{aligned} \dot{d}_e &= \nu \sin(\theta_e), \\ \dot{\theta}_e &= \omega - \frac{\nu \kappa(s) \cos(\theta_e)}{1 - d_e \kappa(s)}. \end{aligned} \quad (34)$$

In equation (34), we have the state variables θ_e , which represents the angle error, and d_e , which represents the

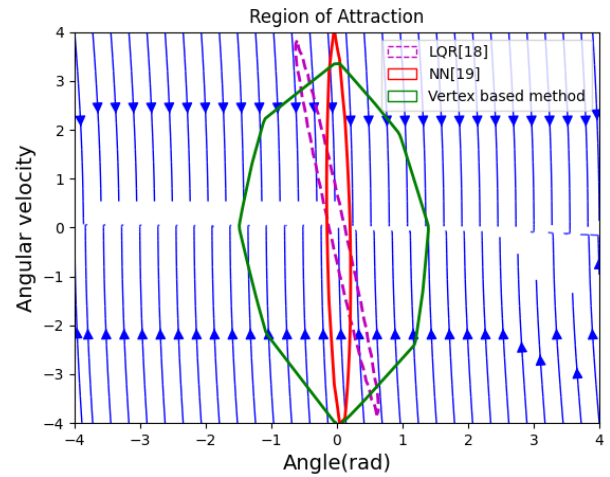


Fig. 9. The ROA for the closed-loop inverted pendulum using LQR [17], NN [18] and vertex-based method.

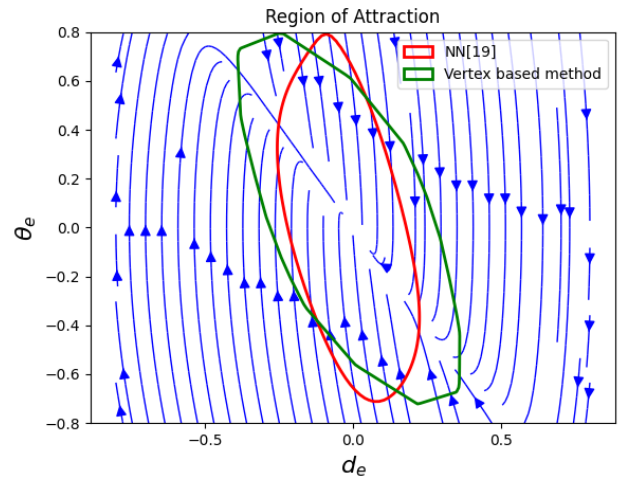


Fig. 10. The ROA for the closed-loop path following wheeled vehicle using NN [18] and vertex-based method.

distance error. The control input is denoted as ω . In this study, we used a single-hidden layer ReLU with 50 neurons as described in [10] in order to identify the dynamic (34) with the NN controller [18] in the region $\|x\|_\infty \leq 0.8$. Moreover, we used the vertex-based method along with vector field refinement to obtain the PWA Lyapunov function. As can be seen in Fig. 10, a comparison was made between the ROA obtained by the proposed method and the ROA obtained using the NN Lyapunov function [18].

Moreover, the computational time for each example is presented in the TABLE I. Having run each simulation ten times, the computational time is the average time elapsed.

VI. DISCUSSION

We have demonstrated the effectiveness of our automated approach to stability verification through examples. We have demonstrated that the proposed refinement methods are superior to those available in the state-of-the-art. Additionally, our

| Example | Average computational time(sec) | | |
|-----------|---------------------------------|----------------|--------------|
| | Naive approach | Lyapunov based | Vector field |
| Example 1 | 0.15 | 0.15 | 0.15 |
| Example 2 | 1.8 | 1.8 | 1.86 |
| Example 3 | 1.27 | 1.27 | 1.29 |
| Example 4 | Failed | 1200 | 280 |
| Example 5 | 23.3 | 17.4 | 16.1 |
| Example 6 | 17.6 | 14.5 | 11.2 |

TABLE I

SUMMARY OF EXAMPLES OF APPLYING THE PROPOSED METHODS.

results demonstrated that, despite the fact that this method is not designed to maximize the region of attraction, its results are comparable with those obtained by other methods. The following sections discuss the challenges associated with making this algorithm applicable to a broader range of problems.

Limitations: To evaluate the computational complexity and performance of our proposed algorithm, it is important to consider the increase in the number of cells and optimization parameters during the refinement process. Generally, in a space \mathbb{R}^n , the number of cells m should satisfy $m \geq 2^n$. In the simplest case, where the origin is surrounded by 2^n simplex cells, the optimization problem will have $2^n \times (n+1)$ parameters and $2^{n+1} \times n$ inequality constraints without considering equality constraints. However, if non-simplex cells are present in the partition, the number of constraints will increase accordingly. For instance, in a 6-D problem, the simplest case involves 448 parameters and 768 inequality constraints at the start of optimization, excluding equality constraints. A large part of the optimization process depends on the n , which significantly influences the problem's computational complexity. As cells are further split, the problem becomes more complex, resulting in longer computational times for optimization. The algorithm may become bogged down in certain cases due to the increased complexity.

To compare the results of different examples in terms of computational time and the number of cells, we introduce the following concepts:

$$T_{\text{opt}_i} = \frac{\sum_{j=1}^i t_{\text{opt}_j}}{\sum_{i=1}^N t_{\text{opt}_i}} \quad (35)$$

$$Nr_i = \frac{n_{r_i}}{\sum_{i=1}^N n_{r_i}} \quad (36)$$

Here, T_{opt} represents the normalized accumulative optimization time, N_r denotes the normalized number of regions, t_{opt} is the time consumed to find the solution using the MOSEK solver, n_r represents the number of regions, and N is the number of iterations required to solve the problem. The subscripts i and j indicate the optimization iteration.

Fig.11. illustrates the relationship between the normalized accumulative optimization time T_{opt} and the normalized number of cells N_r for three different examples. In the case of Example 2 and Example 3, the graph exhibits almost linear behavior. However, in Example 4, the graph demonstrates an

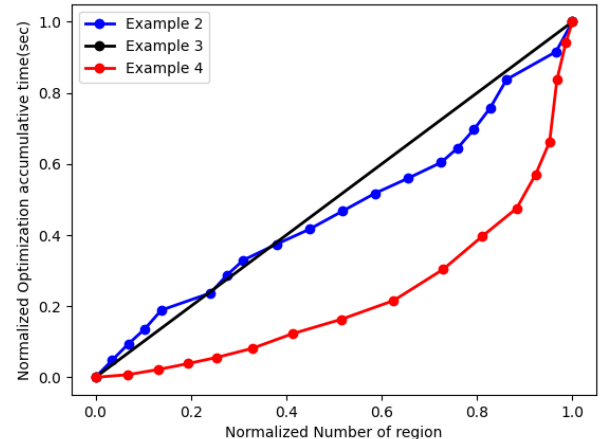


Fig. 11. normalized Accumulative time for optimization vs. the normalized number of regions. The accumulative optimization time with respect to the number of cells for 2-D examples is almost linear; however, in the 4-D example, the accumulative time grows exponentially with respect to the number of cells.

almost exponential trend. Therefore, increasing the number of cells could pose a significant challenge to our proposed technique. Furthermore, the refinement process may lead to cells with nearly coplanar vertices, which can introduce numerical difficulties.

Considering the complexities and challenges associated with the refinement process is crucial when applying our algorithm to different systems.

VII. CONCLUSION

This paper introduces a computational framework for obtaining a PWA Lyapunov function. The PWA Lyapunov function can be derived from applications such as explicit MPC or ReLU neural networks. By formulating the Lyapunov conditions as a linear optimization problem, the PWA Lyapunov function offers a systematic approach for stability analysis. However, it is important to note that the solution to this optimization problem does not always guarantee a valid Lyapunov function. To address this limitation, we propose two novel refinement methods that enhance the flexibility of the candidate Lyapunov function. Additionally, the refinement process is automated using the Delaunay triangulation. The effectiveness of the proposed method is demonstrated through extensive experiments and comparisons with alternative approaches. Specifically, a 4-D example was successfully solved in less than five minutes using the presented method. Comparative analysis with other methods further validates the efficacy and superiority of our approach. Based on the results obtained from these experiments, we conclude that the framework we have proposed is a highly effective tool for generating valid PWA Lyapunov functions. This approach is effective and practical due to the flexibility introduced by refinement methods along with the automated process.

REFERENCES

[1] T. Marcucci, R. Deits, M. Gabiccini, A. Bicchi, and R. Tedrake, “Approximate hybrid model predictive control for multi-contact push recovery in complex environments,” in *2017 IEEE-RAS 17th International Conference on Humanoid Robotics (Humanoids)*. IEEE, 2017, pp. 31–38.

[2] X. Sun, H. Zhang, Y. Cai, S. Wang, and L. Chen, “Hybrid modeling and predictive control of intelligent vehicle longitudinal velocity considering nonlinear tire dynamics,” *Nonlinear Dynamics*, vol. 97, no. 2, pp. 1051–1066, 2019.

[3] M. Johansson, “Piecewise linear control systems,” Ph.D. dissertation, Ph. D. Thesis, Lund Institute of Technology, Sweden, 1999.

[4] A. Bemporad, F. Borrelli, and M. Morari, “Piecewise linear optimal controllers for hybrid systems,” in *Proceedings of the 2000 American Control Conference. ACC (IEEE Cat. No. 00CH36334)*, vol. 2. IEEE, 2000, pp. 1190–1194.

[5] T. Marcucci and R. Tedrake, “Mixed-integer formulations for optimal control of piecewise-affine systems,” in *Proceedings of the 22nd ACM International Conference on Hybrid Systems: Computation and Control*, 2019, pp. 230–239.

[6] J. Qiu, W. Ji, H.-K. Lam, and M. Wang, “Fuzzy-affine-model-based sampled-data filtering design for stochastic nonlinear systems,” *IEEE transactions on fuzzy systems*, vol. 29, no. 11, pp. 3360–3373, 2020.

[7] A. Alessio and A. Bemporad, “A survey on explicit model predictive control,” *Nonlinear Model Predictive Control: Towards New Challenging Applications*, pp. 345–369, 2009.

[8] I. Jebellat, H. N. Pishkenari, and E. Jebellat, “Training microrobots via reinforcement learning and a novel coding method,” in *2021 9th RSI International Conference on Robotics and Mechatronics (ICRoM)*, 2021, pp. 105–111.

[9] Í. Elguea-Aguinaco, A. Serrano-Muñoz, D. Chrysostomou, I. Inziarte-Hidalgo, S. Bøgh, and N. Arana-Arexolaleiba, “A review on reinforcement learning for contact-rich robotic manipulation tasks,” *Robotics and Computer-Integrated Manufacturing*, vol. 81, p. 102517, 2023.

[10] P. Samanipour and H. A. Poonawala, “Stability analysis and controller synthesis using single-hidden-layer relu neural networks,” *IEEE Transactions on Automatic Control*, 2023.

[11] A. Abate, D. Ahmed, M. Giacobbe, and A. Peruffo, “Formal synthesis of lyapunov neural networks,” *IEEE Control Systems Letters*, vol. 5, no. 3, pp. 773–778, 2020.

[12] M. Korda, “Stability and performance verification of dynamical systems controlled by neural networks: algorithms and complexity,” *IEEE Control Systems Letters*, 2022.

[13] H. Ravanbakhsh and S. Sankaranarayanan, “Learning lyapunov (potential) functions from counterexamples and demonstrations,” *arXiv preprint arXiv:1705.09619*, 2017.

[14] M. Farsi, Y. Li, Y. Yuan, and J. Liu, “A piecewise learning framework for control of unknown nonlinear systems with stability guarantees,” in *Learning for Dynamics and Control Conference*. PMLR, 2022, pp. 830–843.

[15] O. Bastani, Y. Ioannou, L. Lampropoulos, D. Vytiniotis, A. Nori, and A. Criminisi, “Measuring neural net robustness with constraints,” *Advances in neural information processing systems*, vol. 29, 2016.

[16] M. Fazlyab, M. Morari, and G. J. Pappas, “Safety verification and robustness analysis of neural networks via quadratic constraints and semidefinite programming,” *IEEE Transactions on Automatic Control*, 2020.

[17] Y.-C. Chang, N. Roohi, and S. Gao, “Neural lyapunov control,” *Advances in neural information processing systems*, vol. 32, 2019.

[18] R. Zhou, T. Quartz, H. De Sterck, and J. Liu, “Neural lyapunov control of unknown nonlinear systems with stability guarantees,” *arXiv preprint arXiv:2206.01913*, 2022.

[19] S. Chen, M. Fazlyab, M. Morari, G. J. Pappas, and V. M. Preciado, “Learning lyapunov functions for hybrid systems,” in *Proceedings of the 24th International Conference on Hybrid Systems: Computation and Control*, 2021, pp. 1–11.

[20] R. R. Bunel, I. Turkaslan, P. Torr, P. Kohli, and P. K. Mudigonda, “A unified view of piecewise linear neural network verification,” *Advances in Neural Information Processing Systems*, vol. 31, 2018.

[21] H. Dai, B. Landry, L. Yang, M. Pavone, and R. Tedrake, “Lyapunov-stable neural-network control,” *arXiv preprint arXiv:2109.14152*, 2021.

[22] R. Iervolino, D. Tangredi, and F. Vasca, “Lyapunov stability for piecewise affine systems via cone-copositivity,” *Automatica*, vol. 81, pp. 22–29, 2017.

[23] R. Iervolino, S. Trenn, and F. Vasca, “Asymptotic stability of piecewise affine systems with filippov solutions via discontinuous piecewise lyapunov functions,” *IEEE Transactions on Automatic Control*, vol. 66, no. 4, pp. 1513–1528, 2020.

[24] J. Anderson and A. Papachristodoulou, “Advances in computational lyapunov analysis using sum-of-squares programming,” *Discrete & Continuous Dynamical Systems-B*, vol. 20, no. 8, p. 2361, 2015.

[25] H. A. Poonawala, “Stability analysis via refinement of piece-wise linear lyapunov functions,” in *2019 IEEE 58th Conference on Decision and Control (CDC)*, 2019, pp. 1442–1447.

[26] —, “Stability analysis of conewise affine dynamical systems using conewise linear lyapunov functions,” in *2021 American Control Conference (ACC)*. IEEE, 2021, pp. 2406–2411.

[27] H. A. Poonawala, N. Lauffer, and U. Topeu, “Training classifiers for feedback control with safety in mind,” *Automatica*, vol. 128, p. 109509, 2021.

[28] M. Henk, J. Richter-Gebert, and G. M. Ziegler, “Basic properties of convex polytopes,” in *Handbook of discrete and computational geometry*. Chapman and Hall/CRC, 2017, pp. 383–413.

[29] H. K. Khalil, *Nonlinear control*. Pearson New York, 2015, vol. 406.

[30] M. Della Rossa, A. Tanwani, and L. Zaccarian, “Smooth approximation of patchy lyapunov functions for switched systems,” *IFAC-PapersOnLine*, vol. 52, no. 16, pp. 364–369, 2019.

[31] R. Baier, L. Grüne, and S. Freyr Hafstein, “Linear programming based lyapunov function computation for differential inclusions,” 2012.

[32] M. El Ghami, Z. Guennoun, S. Bouali, and T. Steihaug, “Interior-point methods for linear optimization based on a kernel function with a trigonometric barrier term,” *Journal of Computational and Applied Mathematics*, vol. 236, no. 15, pp. 3613–3623, 2012.

[33] J. Zago, E. Camponogara, and E. Antonelo, “Vertex-based reachability analysis for verifying relu deep neural networks,” *arXiv preprint arXiv:2301.12001*, 2023.

[34] M. Rubagotti, S. Trimboli, D. Bernardini, and A. Bemporad, “Stability and invariance analysis of approximate explicit mpc based on pwa lyapunov functions,” *IFAC Proceedings Volumes*, vol. 44, no. 1, pp. 5712–5717, 2011.

[35] V. T. Rajan, “Optimality of the delaunay triangulation in rd,” in *Proceedings of the seventh annual symposium on Computational geometry*, 1991, pp. 357–363.

[36] M. ApS, “Mosek optimizer api for python,” *Version*, vol. 9, no. 17, pp. 6–4, 2022.

[37] M. Kvasnica, P. Grieder, M. Baotić, and M. Morari, “Multi-parametric toolbox (mpt),” in *Hybrid Systems: Computation and Control: 7th International Workshop, HSCC 2004, Philadelphia, PA, USA, March 25–27, 2004. Proceedings* 7. Springer, 2004, pp. 448–462.